ChemComm

COMMUNICATION

View Article Online
View Journal | View Issue

Cite this: *Chem. Commun.*, 2025, **61**, 3387

Received 25th December 2024,
Accepted 22nd January 2025

DOI: 10.1039/d4cc06720g

rsc.li/chemcomm

Identification of the Cr(v)=O intermediate in electrocatalytic water oxidation by a chromium(iii)–aqua complex†

Zhi-Kai Shen, Zi-Jian Li, Zhigang Zou and Zhen-Tao Yu *

A new molecular chromium(iii)–aqua catalyst for homogeneous electrocatalytic water oxidation reactions is presented. The key high-oxidation-state Cr(v)–oxo intermediate of water oxidation was identified by HR-MS, EPR, and *in situ* spectroelectrochemistry. Based on DFT calculation, a possible catalytic cycle *via* a WNA pathway was proposed for water oxidation.

Due to the sluggish kinetics, water oxidation is considered to be the bottleneck for the overall efficiency of water splitting.[1] Water oxidation catalysts based on 3d transition metals that operate with high efficiency and stability under mild conditions have attracted much attention in recent years.[2] Group 6 metals (Cr, Mo, W) are often used as doping atoms to optimize the structure of heterogeneous catalysts [*e.g.* (multi)metal oxyhydroxides and oxides],[3] thereby assisting in improving water oxidation activity, but the true role of group 6 metals remains unclear. The study on well-defined molecular structures enables the elucidation of catalytic mechanisms to guide the development of future electrocatalysts, which can be achieved through metal complexes.[4] Besides, it has been shown that the adsorption and activation of water molecules on metal active sites are commonly the initial and key steps for water oxidation.[5] Hence, the metal–aqua complex catalysts provide useful perspectives for directly understanding the reaction mechanism of water oxidation, and a study of this model complex may contribute to designing efficient catalysts.[6]

As a typical 3d metal, chromium (Cr) metal ions have diverse oxidation states (from +1 to +6).[7] This unique property is beneficial for electrocatalysis and has promoted their use in asymmetric catalysis and polymerization catalysis.[8] However, the investigation of Cr-based complexes as water oxidation catalysts is still scarce.[9] The high-oxidation-state metal–oxo species are often proposed as essential intermediates involved in water oxidation.[10] However, the Cr–oxo species are too stable compared with other transition metals (*e.g.* Fe, Co, Ni), thus hindering the subsequent water oxidation steps.[11] In 2018, Pashabadi and coworkers reported an example of a homogeneous {Cr[diphenoxy *N*,*N*′-ethylenebis(salicylimine)-2H]Cl} catalyst for water oxidation with an overpotential of 0.426 V in alkaline solution.[8] However, the origin of the water oxidation activity of Cr complexes is still controversial. Najafpour and coworkers demonstrated that this Cr-based complex transforms into a thin complex-based film during consecutive CVs and thus it has no water oxidation activity.[12] Machan and coworkers indicated that ligand design (*e.g.* polypyridine frameworks) is a feasible way to control the activity of Cr complexes, given the capacity to sterically protect reactive bonds.[13] Therefore, the study of Cr-based complexes with a suitable ligand may improve our understanding of the function of Cr in water oxidation and provide insights into the development of the chemistry of group 6 metals.

Herein, we designed and synthesized a new molecular Cr catalyst (**1**), $CrL(H_2O)(OTf)_3$ (L = H_2bipyalk = 2,2′-([2,2′-bipyridine]-6,6′-diyl)bis(propan-2-ol); OTf = triflouromethanesulfonate), which exhibited attractive activity for water oxidation *via* a water nucleophilic attack (WNA) pathway based on experiments and DFT calculation. The key high-oxidation-state Cr–oxo intermediate during water oxidation was identified by *in situ* spectroelectrochemistry. The isotope experiment proved that the O atoms for O_2 production originated from water. This work provides an entry point for the study and application of group 6 metals in water oxidation.

The molecular structure of **1** was determined by single-crystal X-ray diffraction analysis (Fig. 1b). The Cr–O bond length of 1.974 Å is close to the reported Cr(iii)–O bonds and much shorter than the Cr(iv or v)–O bonds of *ca.* 1.5 Å (Table S2, ESI†).[14] The structure of complex **1** was established by high-resolution atmospheric pressure chemical ionization mass spectrometry in MeCN (APCI-MS, *m*/*z*: $[M + bipyalk]^+$ calcd for 322.0768; found 322.0756, Fig. S1, ESI†). The oxidation state of Cr was confirmed as +3 by normalized Cr K-edge X-ray absorption spectroscopy

National Laboratory of Solid State Microstructures and Jiangsu Provincial Key Laboratory for Nanotechnology, College of Engineering and Applied Sciences, Nanjing University, Nanjing, Jiangsu 210093, People's Republic of China. E-mail: yuzt@nju.edu.cn

† Electronic supplementary information (ESI) available. CCDC 2408326. For ESI and crystallographic data in CIF or other electronic format see DOI: https://doi.org/10.1039/d4cc06720g

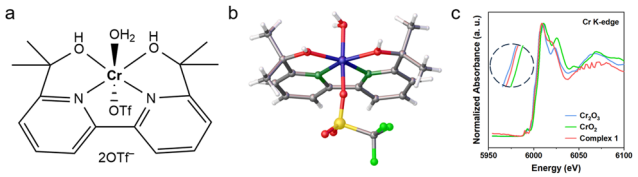

Fig. 1 (a) Schematic representation and (b) X-ray crystal structure showing thermal ellipsoid plot (co-crystallized solvent molecules and counter anions ($2OTf^-$) have been omitted for clarity) of complex **1**. (c) Normalized Cr K-edge XAS spectra of complex **1**, Cr_2O_3 and CrO_2.

(XAS, Fig. 1c), the X-band electron paramagnetic resonance (EPR) spectrum (*vide infra*), and the localized orbital bonding analysis (LOBA, Fig. S10, ESI†). The long-term stability of **1** in aqueous solution and acetonitrile/H_2O mixed solution has been verified by the UV-Vis absorption spectra (Fig. S2, ESI†). In aqueous solution, OTf^- may undergo reversible exchange by water or hydroxide to produce *trans*-$CrL(H_2O)_2$ species.[15]

The cyclic voltammetry (CV) curve of complex **1** exhibited an oxidation wave at E = 0.84 V *versus* ferrocenium/ferrocene (*vs.* Fc^+/Fc) in anhydrous acetonitrile (Fig. S3a, ESI†), which was related to the $Cr^{III/IV}$ couple according to the previous reports on Cr complexes.[12,16] The addition of 10% H_2O in acetonitrile led to a large increase in anodic current at approximately 0.70 V *vs.* Fc^+/Fc (Fig. 2a), and the catalytic current was enhanced with increasing water content (Fig. S3b, ESI†), consistent with the electrocatalytic water oxidation process.[17] We performed water oxidation by replacing the acetonitrile with buffer solution and found a curve-crossing phenomenon in the reverse CV scan (Fig. S3c and d, ESI†). Complex **1** is significantly more active than the corresponding complex $CrL(Cl)_3$ (with onset potential = *ca.* 1.00 V *vs.* Fc^+/Fc), since the latter requires a ligand exchange step to start water oxidation.[18] The onset potential of **1** is comparable to that of reported transition metal-based catalysts and even noble metal catalysts (as compared in Table S3, ESI†).[19] The high oxidizing potential of $Cr^{III/IV}$ or $Cr^{III/V}$ was not found in CV because of the signal overlap with the water oxidation current.[20] Differential pulse voltammetry (DPV, Fig. S4, ESI†) measurement provided evidence for the oxidation of the Cr center. The turnover frequency (TOF) was evaluated as *ca.* 2.9 s^{-1} by plotting i_{cat}/i_p *versus* $\nu^{-1/2}$ using eqn (S5) (Fig. S5, ESI†). To further evaluate the performance of complex **1**, controlled potential electrolysis (CPE) under 1.23 V (*vs.* Fc^+/Fc) using an FTO electrode was performed (Fig. S6a, ESI†). The O_2 evolved during the CPE experiment was quantified with gas chromatography, and the maximum faradaic efficiency of water oxidation was calculated as *ca.* 93%. The results are comparable to those of other reported 3d metal-based complex catalysts.[17] An ^{18}O-labelling experiment by differential electrochemical mass spectrometry (DEMS, Fig. S6b, ESI†) was carried out to identify the oxygen source. The results showed the presence of $^{34}O_2$ (an oxygen atom from **1** or a little $H_2{}^{16}O$ in the $H_2{}^{18}O$ reactant and a second oxygen atom from $H_2{}^{18}O$) and $^{36}O_2$ (both oxygen atoms from $H_2{}^{18}O$), indicating that the oxygen atoms for O_2 production come exclusively from water. A rotating ring-disk electrode (RRDE) experiment exhibited that no current of H_2O_2 oxidation was observed at the Pt ring electrode (Fig. S6c, ESI†), which revealed the high selectivity of the complex **1** in water oxidation. The absence of detected CO_2 in DEMS measurement (Fig. S6b, ESI†) is key evidence for the stability of complex **1** in water oxidation.

Proving the molecular nature of the complex involved in the catalytic process remains a great challenge. Over the course of multiple consecutive CVs of **1**, the shape of the waves and the magnitude of the catalytic current were essentially unchanged (Fig. S7a, ESI†). After multiple CV scans, the electrode was rinsed with acetonitrile and recycled in analogous conditions in the absence of **1**. No discernible catalytic activity was observed after recycling compared with the initial background CV curve (Fig. S7b, ESI†). Stable catalytic current and the inactive electrode after CVs were strong evidence for no active species or film formed at the surface of the electrode. More important is that after long-term CPE, the formation of surface deposits on the electrode was ruled out by X-ray photoelectron spectroscopy (XPS, Fig. S7c and d, ESI†) analysis and electrochemical quartz crystal microbalance (EQCM, Fig. 2c) experiment. No heterogeneous nanoparticles in the electrolyte after water oxidation were detected by dynamic light scattering analysis (DLS, Fig. S7e, ESI†). Those results together indicated that complex **1** is stable in functioning as a molecular electrocatalyst for water oxidation.

The identification of truly active species in catalysis is considered to be essential for homogeneous water oxidation systems.[21] Upon addition of 50 equiv. potassium peroxymonosulfate (oxone) into an acetonitrile solution of complex **1**, APCI-MS revealed a new prominent ion peak with an isotopic pattern at m/z 338.0709, which is attributed to $[M{=}O + bipyalk]^+$ species (calculated m/z of 338.0717, Fig. 3a and Fig. S8, ESI†). Besides, the X-band EPR spectrum of a frozen aqueous solution of complex **1** showed a signal at $g \approx 4.8$ (Fig. 3b bottom), which arises from isolated Cr(III) (S = 3/2) species in a distorted geometry.[22,23] This result is consistent with the DFT calculation (Fig. 4 and Fig. S9, ESI†). Upon adding oxone, the signal of Cr(III) (S = 3/2) disappeared while a strong signal emerged at g = 1.98 (Fig. 3b top), that

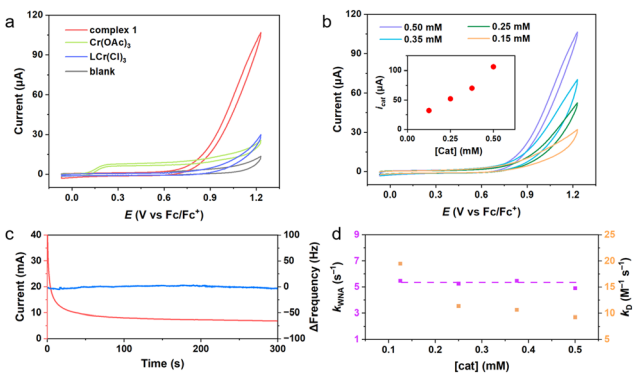

Fig. 2 (a) CVs of 0.5 mM complex **1** in MeCN (0.1 M Et_4NClO_4 as supporting electrolyte) with 10% H_2O. (b) CVs of complex **1** with different concentrations, inset: plot of i_{cat} (current at 1.23 V *vs.* Fc^+/Fc) against [cat.]. Voltammograms were collected on a rotating ring electrode (RDE, GC, 0.2 cm^2, scan rate = 50 mV s^{-1}, rotating rate = 1600 rpm). (c) Results of the EQCM experiment of 0.5 mM complex **1**. (d) Plot of calculated k_D and k_{WNA} *vs.* [cat.] for FOWA.

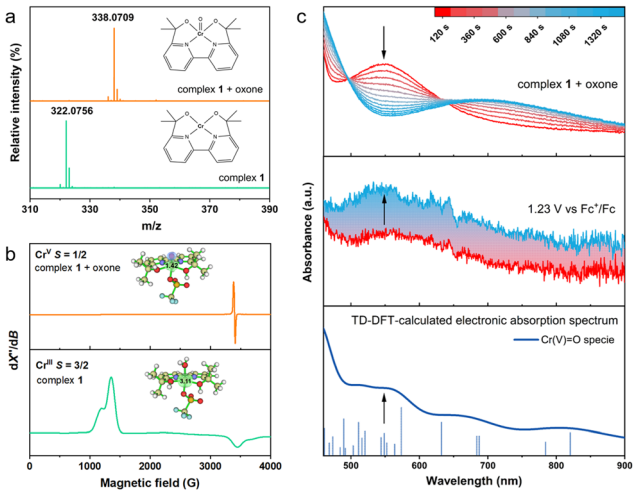

Fig. 3 (a) APCI-MS of complex **1** in MeCN (bottom), and MeCN with 50 equiv. of oxone (top). (b) X-band EPR spectra (at 2 K, microwave frequency = 9.4 GHz) of complex **1** in H_2O (bottom), and H_2O with 50 equiv. of oxone (top). (c) UV-Vis absorption spectra of complex **1**, top: spectra change with time for the reaction of **1** with oxone; middle: spectroelectrochemistry monitoring change during water oxidation at a potential of 1.23 V *vs.* Fc^+/Fc; bottom: TD-DFT-calculated electronic absorption spectrum of the Cr(v)═O intermediate.

is attributed to typical Cr(v) (S = 1/2) species.[24] In UV-vis absorption spectroscopy, a new peak at about λ_{max} = 550 nm appeared after adding oxone (Fig. 3c top). This peak is generally assigned to the high-oxidation-state Cr–oxo intermediate.[25] This assignment was further confirmed by the TD-DFT-calculated electronic absorption spectrum (Fig. 3c bottom). Under controlled-potential electrocatalysis at 1.23 V (*vs.* Fc^+/Fc), a similar peak appeared in the spectroelectrochemical spectrum (Fig. 3c middle), suggesting the formation of the same species (Cr^V═O species) as in chemical oxidization processes.

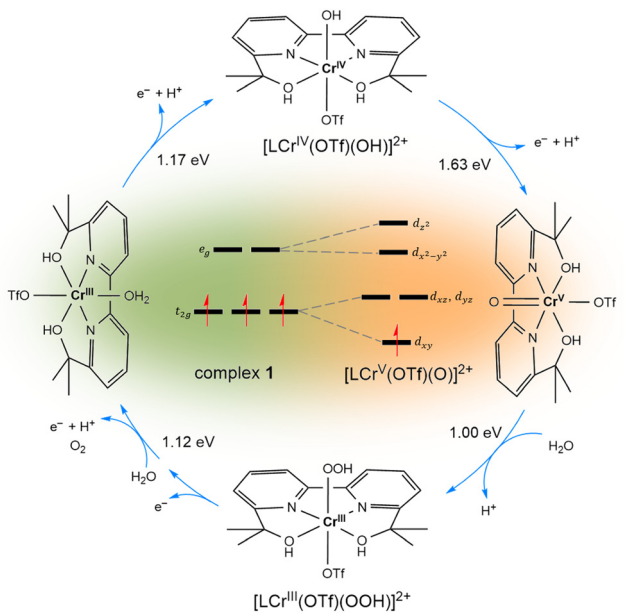

Fig. 4 The proposed catalytic cycle by complex **1**. Electron configuration of 3d electrons in complex **1** and $[LCr^V(OTf)(O)]^{2+}$ species.

A proposed catalytic mechanism by complex **1** is summarized in Fig. 4. The catalytic cycle ensues that Cr–aqua complex **1** undergoes two consecutive one-electron transfers coupled with proton transfer to afford $[LCr^{IV}(OTf)(OH)]^{2+}$ and then reactive $[LCr^{V}(OTf)(O)]^{2+}$ species. The decrease of spin population on Cr in those two steps represents the electron transfer from Cr to OH and the O ligand. The free energy increase for these two steps was calculated to be 1.17 eV and 1.63 eV at the PBE0/def2-TZVP level, respectively. The calculated redox potential for water oxidation is 1.40 V (Fig. S10, ESI†), which is in good agreement with the experimental observation of the onset potential at 0.70 V *vs.* Fc^+/Fc (*ca.* 1.39 V *vs.* NHE). Then, the high-oxidation-state Cr–oxo intermediate undergoes water nucleophilic attack on the Cr═O oxyl species to yield a hydroperoxo $[LCr^{III}(OTf)(OOH)]^{2+}$ intermediate (ΔG = 1.00 eV), which involves the formation of an O–O bond. Next, the $[LCr^{III}(OTf)(OO)]^{2+}$ species is formed with the loss of an electron. This intermediate is further attacked by another H_2O molecule, accompanied by the release of an O_2 molecule and the transformation of electron and proton (ΔG = 1.12 eV). Thus closes the reaction cycle and regenerates the starting complex. The strength of the Cr–O bond is of significance in catalysis since a suitable change in strength favors the activation of water and the release of oxygen.[8] The Cr–O bond length shortens from 2.088 Å to 1.516 Å with the formation of $[LCr^{V}(OTf)(O)]^{2+}$ species (Table S4, ESI†), a typical property of a Cr═O bond (Table S2, ESI†). The shortening of the O–O bond distance from 1.289 Å in $[LCr^{III}(OTf)(OOH)]^{2+}$ to 1.156 Å in $[LCr^{III}(OTf)(OO)]^{2+}$ indicates the formation of a stronger bond between the oxygen atoms, which can be confirmed by the spin density map on $[LCr^{III}(OTf)(OO)]^{2+}$ (Fig. S11, ESI†). Meanwhile, the Cr–O bond is destabilized (increased from 1.516 Å to 2.294 Å) to allow for the scission of the Cr–O bond in $[LCr^{III}(OTf)(OO)]^{2+}$ and release of O_2.

The properties of high-oxidation-state metal–oxo species are important factors that directly affect the water oxidation activity, and the intermediates that are too active or too stable should be avoided.[26] The $[LCr^{V}(OTf)(O)]^{2+}$ intermediate has moderate d electron count and suitable empty d orbitals to accept the electrons of the oxo ligand (Fig. 4 and Fig. S9, ESI†), thus improving the reactivity.[26] Besides, it is reported that the negatively charged ligand is effective to stabilize high-oxidation-state metal–oxo species. The neutral ligand in this work may alleviate the over-stable properties of the intermediate.[27] These two factors work together to ensure the suitable stability and activity of high-oxidation-state Cr–oxo intermediates in our proposed catalytic cycle.

Furthermore, the oxo moiety in the $[LCr^{V}(OTf)(O)]^{2+}$ intermediate with low electron spin density displays no radical character (Fig. S11, ESI†), which effectively reduces the possibility of interaction of two M–O units (I2M) to form a Cr–O–O–Cr intermediate. In experiments, the catalytic currents increased linearly with increasing concentration of **1** (Fig. 2b). The first-order kinetics with respect to the catalyst concentration implied a single-site molecule catalyzing water oxidation.[28] Further analysis of the catalytic water oxidation wave by using foot of the wave analysis (FOWA, Fig. 2d and Fig. S12, ESI†) showed that the observed reaction rate constant (k_{WNA}) remained almost

unchanged at different concentrations of **1**. The dependence of the rate constant on the catalyst concentration and the kinetic isotope effect value (KIE $\approx$ 2.2, Fig. S7f, ESI†) together confirmed the WNA nature of the mechanism operating by complex **1**.[29] Therefore, combining experiments and theoretical calculations, the pathway of O–O bond formation *via* the I2M mechanism can be ruled out in this work. This proposed catalytic cycle further confirms that complex **1** can catalyze water oxidation.

In this work, we have demonstrated that complex **1** is active and stable as a molecular catalyst for homogeneous water oxidation. The key high-oxidation-state Cr–oxo intermediate was identified by the *in situ* spectroscopy technique. Complex **1** started water oxidation without ligand exchange, thus having significantly enhanced water oxidation performance. The presented results may lead to a deep understanding of the electrocatalysis mechanisms, and may also inspire investigation on other group 6 metal (*e.g.* Mo, and W) catalysts.

This work was financially supported by the National Science Foundation of China (Grant No. 22379064) and the National Key R&D Program of China (Grant No. 2021YFF0500502). A portion of this work was performed on the Steady High Magnetic Field Facilities, High Magnetic Field Laboratory, CAS.

Data availability

All relevant data are within the manuscript and its ESI.†

Conflicts of interest

There are no conflicts to declare.

Notes and references

1 Q. Huang, S. Xie, J. Hao, Z. Ding, C. Zhang, H. Sheng and J. Zhao, *Angew. Chem., Int. Ed.*, 2023, **62**, e202300469.
2 L. Zhang, S. Mathew, J. Hessels, J. N. H. Reek and F. Yu, *ChemSusChem*, 2021, **14**, 234–250.
3 B. Zhang, L. Wang, Z. Cao, S. M. Kozlov, F. P. García De Arquer, C. T. Dinh, J. Li, Z. Wang, X. Zheng, L. Zhang, Y. Wen, O. Voznyy, R. Comin, P. De Luna, T. Regier, W. Bi, E. E. Alp, C.-W. Pao, L. Zheng, Y. Hu, Y. Ji, Y. Li, Y. Zhang, L. Cavallo, H. Peng and E. H. Sargent, *Nat. Catal.*, 2020, **3**, 985–992.
4 B. Das, B.-L. Lee, E. A. Karlsson, T. Åkermark, A. Shatskiy, S. Demeshko, R. Liao, T. M. Laine, M. Haukka, E. Zeglio, A. F. Abdel-Magied, P. E. M. Siegbahn, F. Meyer, M. D. Kärkäs, E. V. Johnston, E. Nordlander and B. Åkermark, *Dalton Trans.*, 2016, **45**, 13289–13293.
5 R. Matheu, P. Garrido-Barros, M. Gil-Sepulcre, M. Z. Ertem, X. Sala, C. Gimbert-Suriñach and A. Llobet, *Nat. Rev. Chem.*, 2019, **3**, 331–341.
6 Y. Gao, R. H. Crabtree and G. W. Brudvig, *Inorg. Chem.*, 2012, **51**, 4043–4050.
7 A. D. Bokare and W. Choi, *Environ. Sci. Technol.*, 2011, **45**, 9332–9338.
8 M. Shamsipur, A. Arman Taherpour, H. Sharghi, V. Lippolis and A. Pashabadi, *Electrochim. Acta*, 2018, **265**, 316–325.
9 I. M. Abdullahi and M. Nath, *Catalysts*, 2023, **13**, 721.
10 X. Wei, T. Ding, Y. Wang, B. Yang, Q. Yang, S. Ye, C. Tung and L. Wu, *Angew. Chem., Int. Ed.*, 2023, **62**, e202308192.
11 M. J. McCormick and C. W. Machan, *Dalton Trans.*, 2024, **53**, 16807–16814.
12 N. Akbari and M. M. Najafpour, *Int. J. Hydrogen Energy*, 2021, **46**, 3954–3963.
13 M. E. Moberg and C. W. Machan, *Acc. Chem. Res.*, 2024, **57**, 2326–2335.
14 M. P. Donzello, L. Bartolino, C. Ercolani and C. Rizzoli, *Inorg. Chem.*, 2006, **45**, 6988–6995.
15 C. Godemann, D. Hollmann, M. Kessler, H. Jiao, A. Spannenberg, A. Brückner and T. Beweries, *J. Am. Chem. Soc.*, 2015, **137**, 16187–16195.
16 Q. Liu, A. A. Shinkle, Y. Li, C. W. Monroe, L. T. Thompson and A. E. S. Sleightholme, *Electrochem. Commun.*, 2010, **12**, 1634–1637.
17 Y. Su, W. Luo, W. Lin, Y. Su, Z. Li, Y. Yuan, J. Li, G. Chen, Z. Li, Z. Yu and Z. Zou, *Angew. Chem., Int. Ed.*, 2022, **61**, e202201430.
18 B. Das, A. Orthaber, S. Ott and A. Thapper, *Chem. Commun.*, 2015, **51**, 13074–13077.
19 M. Okamura, M. Kondo, R. Kuga, Y. Kurashige, T. Yanai, S. Hayami, V. K. K. Praneeth, M. Yoshida, K. Yoneda, S. Kawata and S. Masaoka, *Nature*, 2016, **530**, 465–468.
20 D. Wang and J. T. Groves, *Proc. Natl. Acad. Sci. U. S. A.*, 2013, **110**, 15579–15584.
21 D. den Boer, Q. Siberie, M. A. Siegler, T. H. Ferber, D. C. Moritz, J. P. Hofmann and D. G. H. Hetterscheid, *ACS Catal.*, 2022, **12**, 4597–4607.
22 T. Devi, Y. Lee, J. Jung, M. Sankaralingam, W. Nam and S. Fukuzumi, *Angew. Chem., Int. Ed.*, 2017, **56**, 3510–3515.
23 H. Kotani, S. Kaida, T. Ishizuka, K. Mieda, M. Sakaguchi, T. Ogura, Y. Shiota, K. Yoshizawa and T. Kojima, *Inorg. Chem.*, 2018, **57**, 13929–13936.
24 J. Cho, J. Woo, J. Eun Han, M. Kubo, T. Ogura and W. Nam, *Chem. Sci.*, 2011, **2**, 2057–2062.
25 S. Liu, K. Mase, C. Bougher, S. D. Hicks, M. M. Abu-Omar and S. Fukuzumi, *Inorg. Chem.*, 2014, **53**, 7780–7788.
26 B. Zhang and L. Sun, *J. Am. Chem. Soc.*, 2019, **141**, 5565–5580.
27 Q. Zeng, F. W. Lewis, L. M. Harwood and F. Hartl, *Coord. Chem. Rev.*, 2015, **304–305**, 88–101.
28 Q. Chen, Y. Xiao, R. Liao and M. Zhang, *CCS Chem.*, 2023, **5**, 245–256.
29 R. Matheu, S. Neudeck, F. Meyer, X. Sala and A. Llobet, *ChemSusChem*, 2016, **9**, 3361–3369.

